ACS OMEGA

http://pubs.acs.org/journal/acsodf

Article

Paper-Based Platform with an In Situ Molecularly Imprinted Polymer for β-Amyloid

Marta V. Pereira, Ana C. Marques, Daniela Oliveira, Rodrigo Martins, Felismina T. C. Moreira, M. Goreti F. Sales,* and Elvira Fortunato*

Cite This: ACS Omega 2020, 5, 12057−12066

Read Online

ACCESS | Metrics & More | Article Recommendations | Supporting Information

ABSTRACT: Alzheimer's disease (AD) is one of the most common forms of dementia affecting millions of people worldwide. Currently, an easy and effective form of diagnosis is missing, which significantly hinders a possible improvement of the patient's quality of life. In this context, biosensors emerge as a future solution, opening the doors for preventive medicine and allowing the premature diagnosis of numerous pathologies. This work presents a pioneering biosensor that combines a bottom-up design approach using paper as a platform for the electrochemical recognition of peptide amyloid β-42 (Aβ-42), a biomarker for AD present in blood, associated with visible differences in the brain tissue and responsible for the formation of senile plaques. The sensor layer relies on a molecularly imprinted polymer as a biorecognition element, created on the carbon ink electrode's surface by electropolymerizing a mixture of the target analyte (Aβ-42) and a monomer (*O*-phenylenediamine) at neutral pH 7.2. Next, the template molecule was removed from the polymeric network by enzymatic and acidic treatments. The vacant sites so obtained preserved the shape of the imprinted protein and were able to rebind the target analyte. Morphological and chemical analyses were performed in order to control the surface modification of the materials. The analytical performance of the biosensor was evaluated by an electroanalytical technique, namely, square wave voltammetry. For this purpose, the analytical response of the biosensor was tested with standard solutions ranging from 0.1 ng/mL to 1 μg/mL of Aβ-42. The linear response of the biosensor went down to 0.1 ng/mL. Overall, the developed biosensor offered numerous benefits, such as simplicity, low cost, reproducibility, fast response, and repeatability less than 10%. All together, these features may have a strong impact in the early detection of AD.

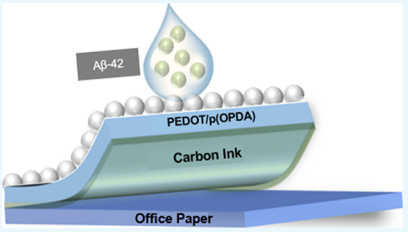

1. INTRODUCTION

Alzheimer's disease (AD) is the most common form of dementia, with 60−80% cases of dementia being attributed to AD and affecting over 45 million people worldwide.[1−3] This neurodegenerative disease is characterized by forgetfulness that evolves into memory loss, behavioral disturbances, and numerous neuropsychiatric episodes.[4] AD is currently uncurable, and its early diagnosis is the best option for a patient, although it is difficult, considering the lack of accurate and effective tests that rely mostly on invasive clinical examination.[5,6]

Recent studies have suggested that AD has systemic signs caused by molecular changes within the disease progression, acting as potential biomarkers. These includes amyloid-β or its derivative compounds,[7] tau/phosphorylated tau protein,[8] BACE1 enzyme,[9] and antibodies,[10] among others. Among these, the relevance of Aβ-42 for AD diagnosis is not questionable, which may be used in isolated form when in cerebrospinal fluid (CSF) or as a ratio when in evaluated serum samples.[7] AD biomarkers can be found in the blood and CSF[11] and until now were detected by complex and expensive techniques such as enzyme-linked immunosorbent assays,[12,13] in vivo positron emission tomography, mass spectrometry, high-performance liquid chromatography,[14] surface plasma resonance,[15−17] field effect transistors,[18] and others.[19] Most of these forms of diagnostics only take in consideration the detection in CSF, which makes them invasive, and some do not allow a point-of-care (POC) analysis.[20] A biosensor that could detect an AD biomarker in blood or urine samples could allow portability, reduction of cost, and an overall easier way to diagnose the disease. In general, a biosensing device integrates a biorecognition element immobilized in a support material, and the interaction between the recognition layer and the target analyte could be transduced by an electrochemical signal.

Electrochemical biosensors show a fast and real-time response, easier miniaturization, portability, low cost, simple procedures, and a wide linear range of detection through the combination of the conventional molecular methods, selectivity, and sensibility related to the signal transduction.[21] Recent developments in the literature report electrochemical bio-

Received: January 20, 2020
Accepted: March 19, 2020
Published: May 15, 2020

https://dx.doi.org/10.1021/acsomega.0c00062
ACS Omega 2020, 5, 12057−12066

Table 1. MIP-Based Electrochemical Biosensors for Aβ-42 Detection[a]

substrate	monomer	technique	sample	LOD	year	refs
Au-WE on ceramic	aniline	EIS/SWV	FBS	420.25 ng/mL (EIS); 0.20 ng/mL (SWV)	2017	36
graphene on GC	pyrrole	CV	breath	0.02 Ppb	2018	37
C-SPE on ceramic	aniline	SWV	cormay Serum	0.40 pg/mL	2018	4

[a]Au-WE: gold WE; C-SPE: carbon screen-printed electrode; GC: glassy carbon; CV: cyclic voltammetry; SWV: square-wave voltammetry; FBS: fetal bovine serum.

sensors for Aβ-42 using enzymes,[22,23] peptides,[24,25] proteases,[26] and mostly antibodies[27−29] for CSF and serum samples. All these elements, and antibodies in particular, show limited stability and high cost.[30] Overall, these handicaps may be eliminated by replacing natural antibodies by synthetic materials that are designed under close-to-native environment conditions and/or reveal great affinity for the molecule of interest. The synthetic solution to mimic natural antibodies relies on using inexpensive polymeric materials, which allow the same required selective recognition, while showing longer stability, which reflects on the shelf life of the devices. Plastic antibodies rely on molecularly imprinted polymer (MIP) technology. MIP materials consist of a three- or two-dimensional (3D or 2D) imprint of a target molecule in a rigid polymeric matrix built with synthetic or natural monomers. The template molecule is later removed without disturbing the geometry of the solid matrix. The exclusion of the target from the polymerized matrix generates imprinted sites that match the size and shape of the target.[31] These imprinted sites are expected to act similar to natural antibodies, rebinding to the target with great affinity and selectivity.[31,32]

Considering that the MIP will be integrated in an electrochemical sensor, the suitable approach for polymer growth is electropolymerization because it allows controlling the film thickness and its morphology.[33,34] In this, the template particles and the monomers are mixed in the same solution and create the polymeric matrix directly on the sensor surface when the required electrical conditions are applied, making biomolecule immobilization and MIP synthesis a one-step process.[35]

There are currently few electrochemical biosensors with MIP materials for AD. Table 1 lists the features of the already developed electrochemical AD biosensors with Aβ-42 as the biomarker. Moreira and Sales[36] in their first MIP-based sensor for AD have achieved a limit of detection (LOD) of 0.20 ng/mL, which was surpassed in their second work,[4] in which they accomplished an LOD value in the pg/mL range (0.40 pg/mL) without the need to incubate an active redox element on the working electrode (WE). Their monomer of choice was aniline, for being stable and easily electropolymerized, much alike phenylenediamine. Emam *et al.*[37] opted for pyrrole, whose electropolymerization conditions are well studied because their MIP-based sensor was very innovative by diagnosing AD in a noninvasive method through the breath of the patient. It is important to highlight that the previously described MIP biosensors, devoted to Aβ-42, may be developed to target other biomarkers circulating in the blood, including Aβ-42 derivatives, most recently established as highly significant in terms of AD.[7] Overall, considering the increasing worldwide incidence of AD, a suitable inexpensive and eco-friendly biosensor with high stability and selectivity is still missing.

The ever-increasing healthcare costs together with the consumer demand, lack of medical care in poor-resource countries, and the constant need for renewable materials are enough reasons to create a new generation of inexpensive, disposable, and less-invasive sensors amenable to mass production to provide the maintenance of welfare, early diagnostics, and medical prevention. These sensors will use low cost and/or flexible materials, such as poly(ethylene terephthalate),[38] print-circuit board,[39] glass, and paper.[40] Among these, paper is easy to fabricate and mass-producible. It has a significantly lower price than plastic substrates, is disposable, and also presents the advantage of being recyclable, while being made from reusable raw materials.[41] So, it makes sense to develop an easy-to-use, rapid, and inexpensive POC device with this substrate.[42,43]

Promising reports of electronic devices fabricated directly onto paper substrates have been recently published.[44,45] Paper has a porous structure and a large surface roughness. It can show fibers with different sizes and shapes, depending on their origin and treatments,[46] but suitable printing schemes enable their easy modification.[47,48] Currently, the few published works that combine plastic antibodies with the electrochemical detection of Aβ-42 have chosen rigid substrates such as glass and ceramic, and therefore this work aims to be the first one to apply this technology on a flexible paper platform.

Plenty of conductive materials can work as electrodes, but the most commonly used is carbon. Carbon comes in numerous varieties of forms and has an extensive application in electrochemical studies. When compared with metal electrodes, carbon has many advantages because of its low cost, wide range of potential windows, and high chemical stability.[49−51] Carbon's most common form is based on the graphite structure, which can be modified or enhanced by surface treatments and modifications and can increase surface roughness, surface area, or oxygenated functional groups on the electrode surface.

The present work describes for the first time a MIP-based electrochemical biosensor for the early diagnosis of AD in a paper-based platform. The biomimetic material consists of a polymeric matrix generated by the electropolymerization of the monomer *O*-phenylenediamine (OPDA) in the presence of the chosen biomarker. To evaluate the success of Aβ-42 imprinting, the electrochemical response of the created devices is compared with nonimprinted polymeric (NIP) materials, which were made in the absence of a template during the electropolymerization step.

2. RESULTS AND DISCUSSION

2.1. Electrodes Pretreatment. A first study was performed to select a suitable pretreatment or cleaning process that would improve the conductivity properties of the carbon electrodes, which presented an initial sheet resistance of 25.69 Ω/square. Readings in blank conditions were done to confirm similarity between several samples. Cyclic voltammetry (CV) and electrochemical impedance spectroscopy (EIS) data (Figure S1) showed the existence of negligible differences.

https://dx.doi.org/10.1021/acsomega.0c00062
ACS Omega 2020, 5, 12057−12066

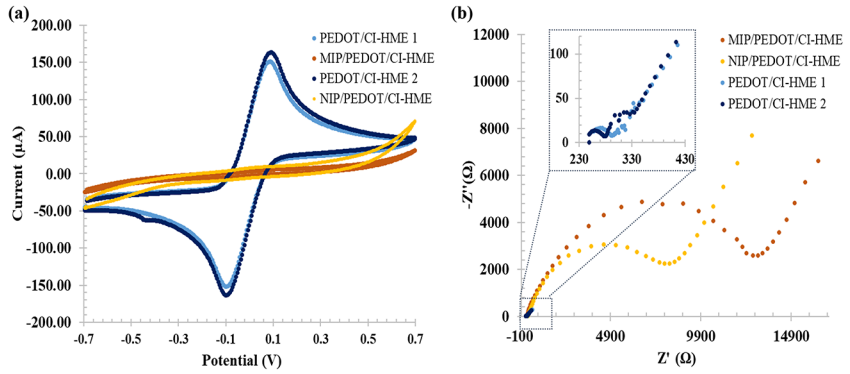

Figure 1. Electrochemical readings of the sensing surfaces (MIP or NIP layers) by (a) CV and (b) EIS before the template removal. Zoomed section represents the sensing surface before electropolymerization (PEDOT layer).

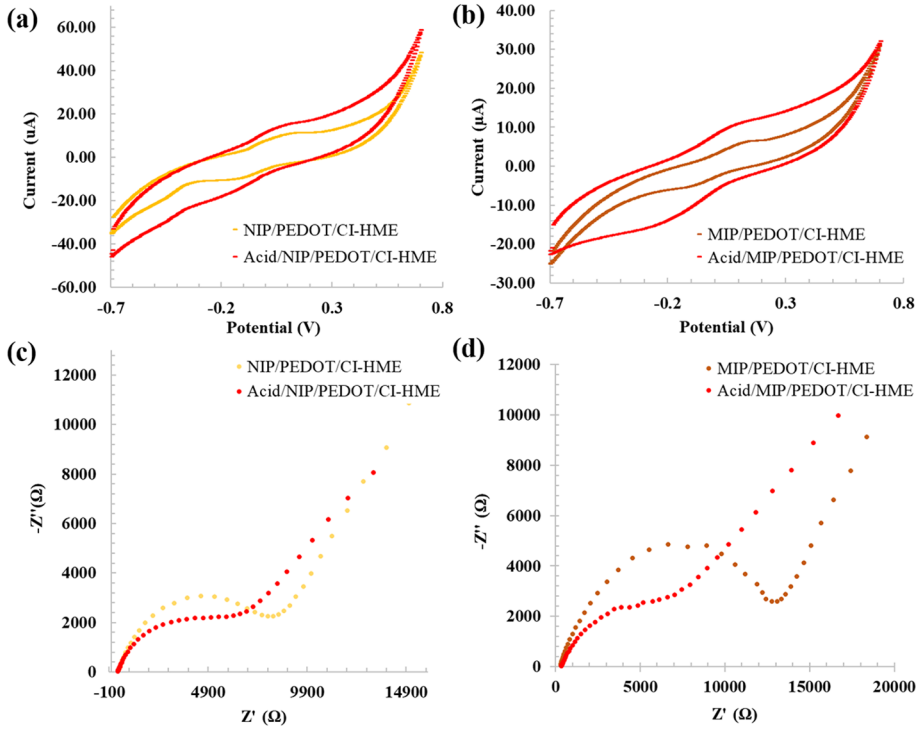

Figure 2. Electrochemical follow-up of the several modification steps of the CI-HME to produce NIP (a,c) and MIP (b,d) films by EIS (c,d, Nyquist plots) and CV (a,b, cyclic voltammograms). Results from a solution of 5.0 mM $[Fe(CN)_6]^{3-}$ and 5.0 mM $[Fe(CN)_6]^{4-}$ in PBS buffer, pH 7.2.

Nonetheless, similar carbon ink homemade electrodes (CI-HMEs) were chosen, and a pretreatment procedure that could work for all was implemented.

In order to get better electrical features, 3,4-3,4-ethylenedioxythiophene (EDOT) modification was selected as the pretreatment stage for CI-HMEs. Such pretreatment stage improved the activity of the electrode by adding a highly conductive polymer layer to the carbon support and by increasing the roughness and number of reactive sites on the electrode surface. For this purpose, the electrodes were treated by chronoamperometry with an EDOT solution for 10 s at 1 V. This potential was selected in agreement with Cardoso *et al.*[35] ensuring that the oxidation potential of EDOT was reached on this surface and that it was not overpassed, which could lead to decomposition of the conductive film.[52] The time for applying this potential followed the studies made in another carbon support tested, as shown in Figure S2.

The improvement of the electrical features is clearly shown in Figure S3. Overall, before pretreatment, no oxidation and reduction peaks were observed within the range of potential applied. This behavior is attributed to the irreversibility of the electrochemical process and the consequent slow rate of the electron charge transfer on the electrode surface.

After poly(3,4-ethylenedioxythiophene) (PEDOT) deposition, it is possible to observe the presence of an oxidation peak (~0.14 V, 125 μA) and reduction peak (~−0.14 V, ~125 μA). The peak separation is ~0.24 V; this process is associated with a quasi-reversible electrochemical process, meaning that the process exhibits a large peak-to-peak separation compared to reversible processes, where it is larger than $0.059/n$.

https://dx.doi.org/10.1021/acsomega.0c00062
ACS Omega 2020, 5, 12057−12066

Yet, these electrical features are, by far, the best conditions obtained with the HMEs and are similar to the electrical features displayed by commercial screen-printed electrodes. Consistently, EIS readings showed very little impedance values, and no charge transfer resistance (R_{ct}) could be extracted from it, evidencing the high conductivity features of the system. The results also pointed out that the applied pretreatment enabled higher homogeneity on the surface by allowing similar results between different batches and a better electrochemical sensor response.

2.2. MIP Fabrication. After the previous pretreatment, the HMEs were incubated in 4-aminothiophenol (ATP) for 1 h. The ATP solution was an intermediate layer between PEDOT and the subsequent *O*PDA layer working as a linker. The thiol group is expected to interact with EDOT, while the amine-aromatic ring should establish a covalent bond with the MIP/NIP film, thereby ensuring that the imprinted polymeric layer was securely bonded to the WE. Considering that this was a spontaneous reaction (no external potential was applied here), it was assumed that the thiol group would form a disulphide bridge with some EDOT molecules on the PEDOT film (maybe those terminating the polymeric structure). Indeed, it was clear that a reaction occurred because the color of the surface changes when the same reaction is tested on an fluorine-doped tin oxde glass support. In turn, after adding ATP, there were functional groups on the surface that could be oxidized by CV (the aromatic amines) for further binding to the subsequent polymeric layer, poly(oPD). Indeed, ATP was found essential to bind steadily the two polymeric layers because without it, the surface became unstable and the electrode would be useless.

After the ATP incubation, the next step was the electropolymerization of *O*PDA (Figure 1). CV was the selected technique for this process, considering the research of Gomes *et al.* 2018[33] and several other papers in the literature using it, even with other monomers.[33] The formation of the *O*PDA film introduced additional barriers to the electron-transfer properties of the redox probe. This resulted in an extra increase in the electron-transfer resistance, reflected by a substantial rise in R_{ct} compared to HMEs in the previous state. The presence of Aβ-42 on the surface of the WE, after its adsorption, was confirmed by an R_{ct} increase compared to the NIP HME-1 (Figure 1B). This upsurge was much more evident in the MIP, reflecting the presence of an insulating film plus the peptide.

For the removal process, the HMEs were incubated in a trypsin solution at 36 °C for 1 h. This step was meant to remove the peptide from its imprinted site, leaving the remaining polymeric network for the artificial antibody. Trypsin is highly active and stable with low cutting specificity and exhibits wide cleavage specificity.

After treatment with trypsin, some HMEs had unstable electrical responses after consecutive readings, which could be due to the adsorption of trypsin into the matrix. Thus, an extra step was added. Another incubation was made using oxalic acid for 2 h to ensure proper protein removal. After template removal, the resistance decreased substantially in the MIP (Figure 2d) and moderately in the NIP (Figure 2c). The variation of R_{ct} for MIP and NIP materials were $\Delta \approx 30$ and 13%, respectively. The higher variation in the MIP sensor is due to the absence of the peptide in the polymeric matrix, once the nature of the polymeric matrix is similar.

In general, this overall decrease accounted for the eventual removal of adsorbed trypsin and small oligomeric fragments, both in MIP and NIP films. The substantial decrease in the MIP (Figure 2d) reflected the exit of the AD peptide from the polymeric network.

CV assays (Figure 2a,b) were consistent with the EIS results. The redox probe showed typical peak-to-peak potential separation values on both devices with EDOT. The subsequent adsorption of the protein promoted a peak decrease and a potential shift to higher values, confirming the presence of an additional element on the WE. After the polymerization, the peak currents dropped to lower levels, confirming the formation of an insulating layer on top of the HME surface. After template removal, the peak currents recovered, confirming the exit of the peptide from the electrode's surface. The NIP values showed similar behavior, except after polymerization, where the redox peaks of the probe remained evident.

2.3. Surface Characterization. The morphological and chemical characterization of the biomimetic materials as well as the control films were made through scanning electron microscopy (SEM), Raman spectroscopy, and atomic force microscopy (AFM) analyses.

2.3.1. Raman Spectroscopy Analysis. Raman spectra were recorded for each different stage of construction of the sensing film (Figure 3). In general, Raman spectra revealed the

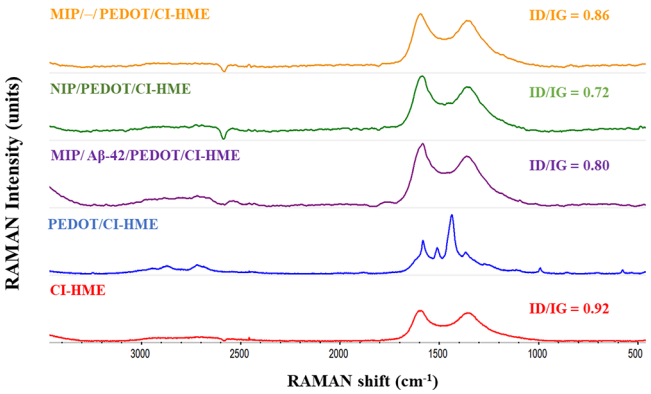

Figure 3. Raman Spectra of CI-HME, PEDOT/CI-HME, MIP/Aβ-42/PEDOT/CI-HME, NIP/PEDOT/CI-HME, and MIP/-/PEDOT/CI-HME.

presence of a carbon-based matrix by showing two prominent visible peaks (D and G) at 1350 and 1580 cm^{-1} because all materials relied on a carbon background. The G peak represented the bond-stretching vibrations of sp^2 hybridization carbon atoms expressing the C=C stretching; the D peak expressed the vibrations of the carbon atoms of dangling bonds or sp^3 hybridization of carbon atoms, indicating the presence of disordered and/or defected in the carbon. The 2D peak represented the second order of the D band, involving a two-phonons lattice vibrational process, without the presence of any kind of disorder or defects.[53]

In general, the intensity ratio (I_D/I_G) is characteristic of the extent of disorder present within the material: the higher the ratio, the lower the disorder.[54] The CI-HME was the starting material with a ratio of 0.92. The EDOT pretreatment created two additional peaks, the strongest one at 1442.5 cm^{-1} and the other at 1506.2 cm^{-1}, assigned to the C=C stretching and confirming the presence of PEDOT on top of the carbon electrode.[53,55,56] The addition of a polymeric imprinted layer on the PEDOT is expected to contribute to disorder the sp^2

https://dx.doi.org/10.1021/acsomega.0c00062
ACS Omega 2020, 5, 12057−12066

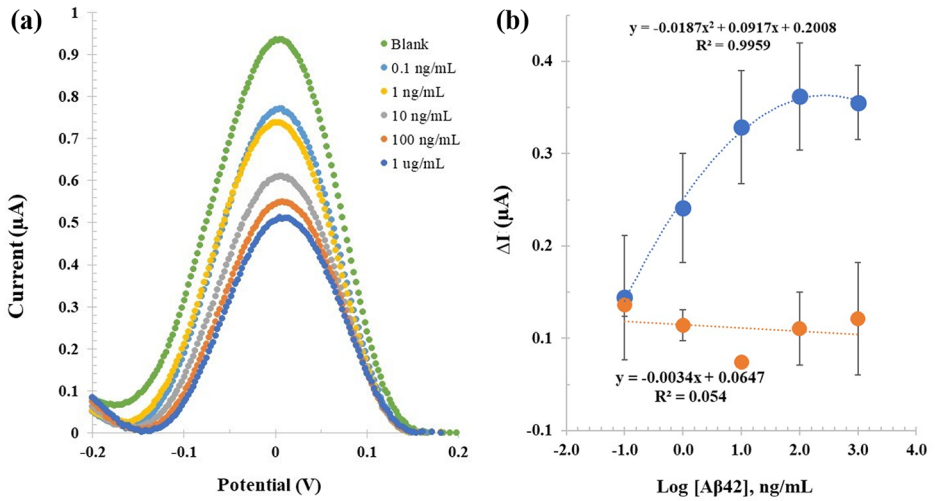

Figure 4. SWV measurements of the (a) MIP/CI-HME-based biosensor and the corresponding calibration curve (b) and MIP (blue dots) and NIP sensing layer (orange dots) calibration curve. Different concentrations of Aβ-42 (ng/mL) in PBS buffer. All assays were performed in 5.0 mM $[Fe(CN)_6]^{3-}$ and 5.0 mM $[Fe(CN)6]^{4-}$ in PBS buffer, pH 7.2.

carbon system, leading to higher ratio, as seen in the MIP/Aβ-42/PEDOT/CI-HME spectrum. The increase of the I_D/I_G ratio from 0.8 to 0.86 was promoted by the removal of the peptide, indicating a higher presence of defects in the structure, which are consistent with the template sites present in the MIP structure. The NIP showed the lowest ratio because of the absence of imprinted sites and therefore the lowest defects in the structure. Overall, the surface modifications and the presence of imprinting sites on the sensor were confirmed by these results.

2.3.2. SEM Analysis. SEM images were collected during several construction stages showing, in general, visible changes in the WE for each modification. The first one, the EDOT pretreatment displays a noticeable smooth film on the surface (comparing to the as-produced electrodes) that not only increased the electrode's conductivity but also created an even layer for the electrochemical steps further ahead (Figure S4a,b). After polymer growth, the NIP (Figure S4c) and MIP (Figure S4d) images look quite similar, with the MIP showing less empty spaces, probably associated with the presence of the peptide. After template removal, it was possible to identify several empty spaces on the surface of the WE (Figure S4e).

2.3.3. AFM Analysis. The morphological features resulting from each modification stage were studied on the CI-HME surface by AFM analysis. This surface revealed to be highly rough (Figure S5a) because the ink was deposited by homemade approaches; so consequently, the detection of any morphological changes promoted by single monolayer modification was very difficult to observe. Nevertheless, it is possible to follow the different events of the biosensor's construction by the different RMS (root mean square) values of each surface modification. The electropolymerization of EDOT on top of the carbon electrode renders a smoother film, which is confirmed by the decrease of the RMS from 60.2 to 1.42 nm (which is in accordance with the SEM image), allowing a superficial roughness low enough to allow the detection of changes related to the subsequent chemical modification (Figure S5b). The electropolymerization and subsequent formation of the MIP (Figure S5c) rendered significant changes in the surface roughness, which increased up to 71.43 nm because of the addition of a 3D polymeric monolayer onto the WE surface that grows around the template. After the treatment with trypsin and acid, surface roughness increased to 98.04 nm, confirming the exit of the peptide and the presence of the template sites (Figure S5d). With the addition of Aβ-42, these sites are no longer empty and the surface roughness decreased to 58.48 nm (Figure S5e), which is consistent with the calculation method employed in RMS that calculates the arithmetic mean of the squares of a set of numbers. Regarding the NIP formation, as expected, the RMS is lower than that of the MIP (68.29 nm instead of 71.43 nm) because of the absence of the template.

2.4. General Analytical Features. *2.4.1. Calibration Curves in Buffer.* Some controversy still exists regarding the amounts of Aβ-42 present in healthy and AD patients; therefore, this work considered 23.3 pg/mL as the close value displayed by a healthy individual.[57] To test the analytical performance of the biosensor, calibration curves were recorded to demonstrate the ability of the proposed device to recognize the target biomarker, relying on the high affinity recognition cavities in the MIP materials. The analytical response was tested in phosphate-buffered saline (PBS) buffer under similar-to-physiological conditions, pH 7.2.

The SWV current responses were measured after each standard concentration was allowed to bind to the sensing layer for a fixed period of 20 min, as shown in Figure 4a. The typical calibration curves so obtained are shown in Figure 4b, expressing log concentration against the relative values to the blank signal.

The oxidation/reduction current responses of the iron redox probe in the MIP devices were inversely proportional to the Aβ-42 concentration. In general, the peak current at 0 V decreased with increasing concentrations of Aβ-42 diluted in PBS. The incubation with the lowest standard solution dropped the current values significantly, whereas the last three exhibited a little variation of the current, pointing out a tendency for saturation. Under optimized conditions, the MIP exhibited a dynamic response range between 0.10 ng/mL and 1.0 μg/mL.

When compared to the MIP sensor, the NIP did not show a linear response to the target analyte in all range of concentrations studied, meaning that the main binding

https://dx.doi.org/10.1021/acsomega.0c00062
ACS Omega 2020, 5, 12057−12066

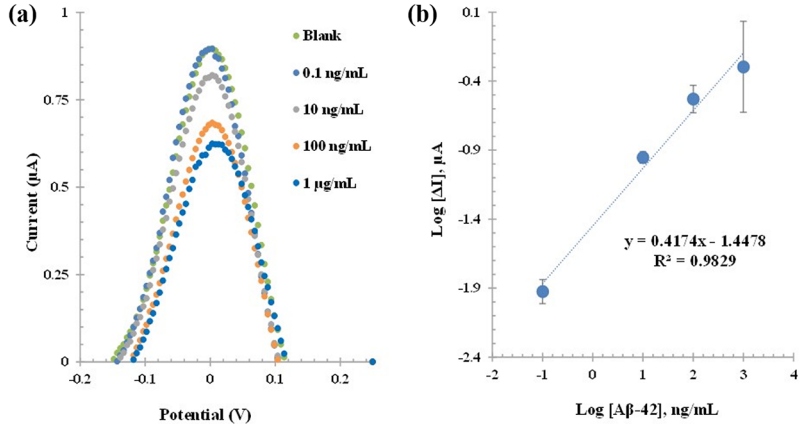

Figure 5. SWV measurements of the (a) MIP/CI-HME-based biosensor in different concentrations of Aβ-42 (ng/mL) in Cormay Serum and the corresponding calibration curve (b, in blue) also compared to the NIP (b, orange). All assays were performed in 5.0 mM $[Fe(CN)_6]^{3-}$ and 5.0 mM $[Fe(CN)_6]^{4-}$ in PBS buffer, pH 7.2.

mechanism was associated with the presence of the cavities (positions acting as plastic antibody) within the polymeric matrix.

2.4.2. Calibration Curves in Serum. In terms of the background medium, the occurrence of Aβ-42 in the CSF and its relation to AD has been established so far, but its presence in the serum emerges now as a possible less-invasive approach. This justifies the selection of serum to test the applicability of this biosensor. Herein, commercial serum was used, which is a highly complex matrix with the ability to produce valuable data regarding the selectivity of the biosensor under conditions of real sample analysis.

Calibration assays conducted in fetal bovine serum (FBS) followed the same process, and the obtained results are seen in (Figure 5).

The MIP was incubated first in serum and later in increasing concentrations of the peptide prepared in serum. In FBS serum samples, considering the blank incubations, no change in the peak current happened for the first standard solution of Aβ-42 compared to the initial reading. Then, the signal decreased with the increase in the concentration of the peptide. Under optimized conditions, the MIP exhibited a dynamic response range between 0.10 ng/mL and 1.0 μg/mL with LOD 0.067 ng/mL.

Overall, these results seemed promising for direct applications in the POC context because within the concentration range observed, the response of the MIP was dominated by the interaction of Aβ-42 with the rebinding sites, with negligible nonspecific response observed.

2.4.3. Selectivity Study. The study of the MIP/CI-HME biosensor is fundamental for an effective analytical application and was evaluated by SWV measurements. The interfering species tested selected were based on the composition of serum samples, such as bovine serum albumin (BSA), glucose (Glu), and creatinine (Crea). Good selectivity was achieved when the sensor was incubated for 20 min each with interfering species. Each assay was conducted in a different MIP/CI-HME in order not to avoid a cross-contamination from the prior adsorbed interfering compound. All species showed negligible effect on the sensory surface compared with Aβ-42 (27%). The percentages for each interfering species was 3, 1, and 0% for BSA, glu, and Crea, respectively. Please see Figure S6.

3. EXPERIMENTAL SECTION

3.1. Reagents and Solutions. All chemicals were of analytical grade and used as supplied without further purification. Milli-Q laboratory grade ultrapure water (conductivity <0.1 μS/cm) was used to prepare all solutions, and all buffer solutions were prepared in PBS (1.0×10^{-2} mol/L, pH 7.36). Potassium hexacyanoferrate III ($K_3[Fe(CN)_6]$) and potassium hexacyanoferrate II ($K_4[Fe(CN)_6]$) trihydrate were purchased from Riedel-de Häen; PBS was purchased from Amresco; potassium chloride (KCl) and oxalic acid dihydrate were purchased from Merck; ethanol absolute (99.5%) was purchased from PanReac; EDOT 97% was purchased from Alfa Aesar; FBS and ATP 96% were purchased from Acros Organics; β-amyloid$^{1-42}$ human (≥95%) was purchased from GenScript; and trypsin solution 10×, *O*PDA, BSA, Crea, and Glu were purchased from Sigma-Aldrich.

The electrical features of the sensing surface were followed by checking the electrical features of a standard redox probe composed of 5.0×10^{-3} mol/L $K_3[Fe(CN)_6]$ and $K_4[Fe(CN)_6]$ prepared in PBS buffer. A KCl solution of 0.1 mol/L was prepared in deionized water. This solution was used as the solvent of an EDOT solution of 0.01 mol/L. A 5.0×10^{-3} mol/L solution of ATP was prepared in a 30% ethanol aqueous solution. *O*PDA standard solutions of 5.0×10^{-5} mol/L were prepared in PBS buffer.

To prepare a control sensing layer (NIP), the polymer was formed in the absence of the target protein. For this purpose, an *O*PDA solution of 50 μmol/L was electropolymerized. The MIP sensing layer was prepared similarly by adding 10 μL of a solution of Aβ-42 (10 μg/mL in PBS buffer, pH 7.36) to 990 μL of the previous solution.

Calibrating solutions required the preparation of stock solutions of Aβ-42 oligomer. These were prepared in a concentration of 0.5 mg/mL in PBS buffer, pH 7.2. The Aβ-42 oligomer was prepared according to Gobbi *et al.*,[58] where the monomeric peptide solutions were diluted to 1.0×10^{-4} mol/L in 5.0×10^{-2} mol/L phosphate buffer and 1.5×10^{-1} mol/L NaCl, pH 7.4 and incubated for 24 h at 4 °C. Less concentrated standards were obtained by accurate dilution of the previous solution in PBS buffer or in Cormay Serum.

For template removal, two solutions were used: trypsin diluted 100× in PBS buffer and oxalic acid 0.05 mol/L prepared in deionized water.

https://dx.doi.org/10.1021/acsomega.0c00062
ACS Omega 2020, 5, 12057−12066

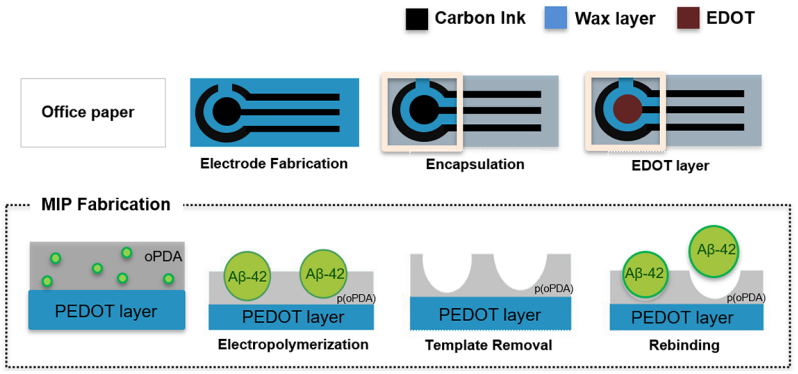

Figure 6. Schematic workflow for MIP production on carbon-ink electrodes prepared on a paper support. OPDA is the monomer used herein, and Aβ-42 is the target biomarker.

3.2. Electrode Fabrication. For the fabrication of the carbon electrodes, paper was the chosen novel support; but since many types of paper exist, office paper (Navigator, 80 g/m^2, 210 × 297 mm sheets) was picked as the best match for electrochemical sensing applications because its surface was suitable for printing. A classical three-electrode configuration was applied for the construction of the biosensor. Because of this application, the paper needed to show hydrophobic behavior, for which a wax treatment was carried out with a Xerox ColorQube 8570 wax printer.[47] After printing, hot plate treatment was performed for 2 min at 120 °C to allow the wax to diffuse throughout the paper thickness, rendering a hydrophobic platform suitable for electrochemical measurements.

Carbon ink (surface resistivity <30 Ω/square), obtained from Conductive Compounds, was used to fabricate the printed carbon electrodes. The paper-based electrochemical devices were prepared by laminating with plastic sheets, previously patterned with a three-electrode architecture, and then coated with two layers of commercial carbon ink, followed by hot plate treatment for 20 min at 120 °C. Along its study, the electrodes were named CI-HMEs. All three electrodes had the same ink material in the final device, shown possible in ref 59 and used without further modification.

3.3. Biosensor Fabrication. Every assay was run in triplicate. The first procedure in each paper-based device was related to the reading of a blank signal (only buffer), and analytical data was presented as relative signal to this blank. The implemented procedures depended on the assembly of the biosensor, described next.

3.3.1. Electrochemical Measurements and Procedures. Electrochemical measurements were performed using a Metrohm Autolab potentiostat/galvanostat PGSTAT320N equipped with a FRA2 module and controlled by NOVA 1.10 software.

CV and SWV measurements were conducted in the standard iron redox probe. For CV assays, the potential was scanned from −0.7 to +0.7 V at 50 mV/s. For SWV studies, potentials ranged from −0.4 to +0.3 V at a frequency of 10 Hz, with a step height of 250 mV. EIS assays were performed with the same redox couple solution $[Fe(CN)^6]^{3-/4-}$ with an open potential circuit using a sinusoidal potential perturbation with an amplitude of 0.01 V and the number of frequencies equal to 50, logarithmically distributed over a frequency range of 0.1−100 kHz. The impedance data was fitted with commercial software Nova.

3.3.2. MIP Assembly. After the first readings, a pretreatment was conducted by chronoamperometry, applying +1 V for 10 s in the EDOT solution. Another reading was made to ensure that the layer of PEDOT was well-formed on the WE. Then, the device was incubated in ATP for 1 h. After this incubation stage, electropolymerization was made by CV with either MIP or NIP preparing solutions. The potentials were scanned from −0.45 to +0.8 V at 100 mV/s in five consecutive cycles. The template removal procedure was made (in both, MIP and NIP sensing layers) by incubating the device in trypsin solution for 90 min at 36 °C, followed by another incubation in oxalic acid for 2 h at room temperature (Figure 6).

3.3.3. Calibration Curve. The calibration curve was performed by SWV and EIS measurements. Readings were measured for MIP and NIP materials, with each assay performed at least three times. Each calibration curve was achieved after a 20 min incubation period for each Aβ-42 standard solution in increasing concentrations. Each Aβ-42 incubation was followed by an iron redox probe reading, extracting the electrical features of the surface for each standard concentration. The Aβ-42 concentrations ranged from 0.1 ng/mL to 1.0 μg/mL prepared in PBS buffer.

Calibration assays were also conducted by incubating Aβ-42 standard solutions prepared in serum, followed by SWV measurements. For this purpose, Aβ-42 was prepared in a Cormay serum solution, diluted 100 times in the same concentration range as before.

3.3.4. Selectivity Study. The selectivity study was performed by incubating the interfering species in the imprinted electrode surface for 20 min. The selected interfering species used were BSA (0.4 mg/mL), Glu (0.7 mg/mL) and Crea (1 μg/mL) solutions prepared in buffer.

3.4. Qualitative Characterization of the MIP Films. The chemical/physical data of the synthetic materials was obtained by surface and chemical analyses using Raman spectroscopy, SEM, and AFM. The samples considered for this study were PEDOT/CI-HME, MIP/PEDOT/CI-HME, trypsin/MIP/PEDOT/CI-HME, and NIP/PEDOT/CI-HME.

Raman spectroscopy data was generated by a Thermo Scientific DXR Raman spectroscope equipped with a confocal microscope and a 532 nm laser. A 5 mW laser power at the sample was allowed for 25 μm slit aperture, 60 s exposure time, and 2 accumulations.

SEM studies were performed on a FE-Cryo SEM/EDS from JEOL JSM 6301F, Oxford INCA Energy 350, and Gatan Alto

https://dx.doi.org/10.1021/acsomega.0c00062
ACS Omega 2020, 5, 12057−12066

2500 microscopes operating at 15 kV and 9.9 mm working distance.

AFM measurements were performed in an Asylum Research MFP-3D Standalone operated in the alternate contact mode in air (commonly known as the tapping mode) using commercially available silicon AFM probes (Olympus AC160TS; k = 26 N/m, f_0 = 300 kHz). The resulting topographies were plane-fitted in Igor Pro software (Wavemetrics), and the final images were generated using Gwyddion software. The roughness (RMS) was automatically calculated in Gwyddion software using the complete 2 × 2 micrometer images. The roughness (RMS) was automatically calculated in Gwyddion software using the complete 2 × 2 micrometer images.

4. CONCLUSIONS

Paper-based diagnostics have been gaining importance in the medical field, particularly regarding clinical analysis applications. Paper is the perfect material to fabricate tailor-made miniaturized electrodes for disposable analytical tests because it is cheap, eco-friendly, disposable, and widely available.

The present work shows a novel combination of a paper-based electrochemical biosensor with molecular imprinting technology for the detection of the peptide Aβ-42, which will allow the early diagnosis of AD. The electrochemical sensor was incorporated with a MIP because it is an alternative approach to natural antibodies. This MIP offers many advantages when compared to natural antibodies, considering its high chemical stability, overall easy fabrication, and low production costs.

Detection of amyloid-β with a MIP-based electrochemical sensor has been reported in the literature (Moreira *et al.*, 2017) but neither on a paper solid substrate, with electropolymerization of OPDA, nor with homemade carbon electrodes. The sensor showed good operational characteristics in the range of 0.1 ng/mL to 1 μg/mL. It showed reproducibility, good response time (around 20 min), and selectivity. As for analytical performance, the biosensor showed adsorption of the peptide within the desired physiologic parameters, considering that a healthy individual shows values close to 23.3 pg/mL.

In general, the presented biosensor showed simplicity in design and short measurement time; taking into account its production, because it has printed carbon electrodes, it is eco-friendly and an outstandingly inexpensive device, around 0.03€ per sensor. This promising new approach opens the doors for the rapid and easy detection of biomarkers associated with AD or other diseases in care settings. In the specific application of AD, it is likely that an array of biosensors may turn out necessary to provide valuable clinical data in serum from suspected patients.

ASSOCIATED CONTENT

Supporting Information

The Supporting Information is available free of charge at https://pubs.acs.org/doi/10.1021/acsomega.0c00062.

Electrochemical comparison between chips; CV measurements before and after electropolymerization of the PEDOT layer; study through CV on the pretreatment of the electrodes; SEM and AFM analyses of the electrode's surface for different steps of construction; and selectivity studies of the developed biosensor (PDF)

AUTHOR INFORMATION

Corresponding Authors

M. Goreti F. Sales − *BioMark, Sensor Research/ISEP, School of Engineering, Polytechnic Institute Porto, 4249-015 Porto, Portugal; CEB, Centre of Biological Engineering Minho University, 4710-957 Braga, Portugal;* orcid.org/0000-0001-9936-7336; Phone: +351228340544; Email: goreti.sales@gmail.com, mgf@isep.ipp.pt; Fax: +351228321159

Elvira Fortunato − *i3N/CENIMAT, Department of Materials Science, Faculty of Science and Technology, Universidade NOVA de Lisboa and CEMOP/UNINOVA, 2829-516 Caparica, Portugal;* orcid.org/0000-0002-4202-7047; Phone: +351212948562; Email: emf@fct.unl.pt; Fax: +351212948558

Authors

Marta V. Pereira − *BioMark, Sensor Research/ISEP, School of Engineering, Polytechnic Institute Porto, 4249-015 Porto, Portugal; CEB, Centre of Biological Engineering Minho University, 4710-957 Braga, Portugal; i3N/CENIMAT, Department of Materials Science, Faculty of Science and Technology, Universidade NOVA de Lisboa and CEMOP/UNINOVA, 2829-516 Caparica, Portugal*

Ana C. Marques − *BioMark, Sensor Research/ISEP, School of Engineering, Polytechnic Institute Porto, 4249-015 Porto, Portugal; i3N/CENIMAT, Department of Materials Science, Faculty of Science and Technology, Universidade NOVA de Lisboa and CEMOP/UNINOVA, 2829-516 Caparica, Portugal*

Daniela Oliveira − *BioMark, Sensor Research/ISEP, School of Engineering, Polytechnic Institute Porto, 4249-015 Porto, Portugal; CEB, Centre of Biological Engineering Minho University, 4710-957 Braga, Portugal*

Rodrigo Martins − *i3N/CENIMAT, Department of Materials Science, Faculty of Science and Technology, Universidade NOVA de Lisboa and CEMOP/UNINOVA, 2829-516 Caparica, Portugal*

Felismina T. C. Moreira − *BioMark, Sensor Research/ISEP, School of Engineering, Polytechnic Institute Porto, 4249-015 Porto, Portugal; CEB, Centre of Biological Engineering Minho University, 4710-957 Braga, Portugal*

Complete contact information is available at: https://pubs.acs.org/10.1021/acsomega.0c00062

Author Contributions

The manuscript was written through contributions of all authors. All authors have given approval to the final version of the manuscript.

Notes

The authors declare no competing financial interest.

ACKNOWLEDGMENTS

The authors acknowledge funding from project PTDC/AAG-TEC/5400/2014, POCI-01-0145-FEDER-016637, POCI-01-0145-FEDER-007688, and UID/CTM/50025/2019 funded by European funds through FEDER (European Funding or Regional Development) via COMPETE2020—POCI (operational program for internationalization and competitively) by national funding through the National Foundation for Science and Technology, I.P. (FCT-MCTES). Additionally, they are grateful to the project IBEROS, Instituto de Bioingenieria en

Red para el Envejecimiento Saludable, POCTEP/0245-BEROS-1-E, PROGRAMA INTERREG 2014-2020 funded through FEDER within the cooperation region of Galiza/Spain and North of Portugal. A.C.M. and F.T.C.M. gratefully acknowledges FCT-MCTES for the financial support (PhD grant reference SFRH/BD/115173/2016 intituled "Nano-biosensing platform based on MIP-SERS for breast cancer exosome characterization and detection" and Post-Doc grant reference SFRH/BPD/97891/2013 intituled "Biomedical devices for easier and quicker screening procedures of the Alzheimer's). This work is part of the Master Thesis in Micro and Nanotechnology Engineering defended by Marta V. Pereira. at FCT NOVA titled "*Fabrication of 3D electrodes for biosensor applications*" in December 2018.

REFERENCES

(1) Murphy, M. P.; LeVine, H., III Alzheimer's Disease and the Amyloid-Beta Peptide. *J. Alzheimer's Dis.* **2010**, *19*, 311−323.
(2) Alzheimer's Association. 2016 Alzheimer's Disease Facts and Figures. *Alzheimer's Dementia* **2016**, *12*, 459−509.
(3) Wimo, A.; Winblad, B.; Aguero-Torres, H.; Von Strauss, E. The Magnitude of Dementia Occurrence in the World. *Alzheimer Dis. Assoc. Disord.* **2003**, *17*, 63−67.
(4) Moreira, F. T. C.; Rodriguez, B. A. G.; Dutra, R. A. F.; Sales, M. G. F. Redox Probe-Free Readings of a B-Amyloid-42 Plastic Antibody Sensory Material Assembled on Copper@carbon Nanotubes. *Sens. Actuators, B* **2018**, *264*, 1−9.
(5) Tierney, M. C.; Fisher, R. H.; Lewis, A. J.; Zorzitto, M. L.; Snow, W. G.; Reid, D. W.; Nieuwstraten, P. The NINCDS-ADRDA Work Group Criteria for the Clinical Diagnosis of Probable Alzheimer's Disease: A Clinicopathologic Study of 57 Cases. *Neurology* **1988**, *38*, 359.
(6) Rushworth, J. V.; Ahmed, A.; Griffiths, H. H.; Pollock, N. M.; Hooper, N. M.; Millner, P. A. A Label-Free Electrical Impedimetric Biosensor for the Specific Detection of Alzheimer's Amyloid-Beta Oligomers. *Biosens. Bioelectron.* **2014**, *56*, 83−90.
(7) Nakamura, A.; Kaneko, N.; Villemagne, V. L.; Kato, T.; Doecke, J.; Doré, V.; Fowler, C.; Li, Q.-X.; Martins, R.; Rowe, C.; et al. High Performance Plasma Amyloid-β Biomarkers for Alzheimer's Disease. *Nature* **2018**, *554*, 249−254.
(8) Mantzavinos, V.; Alexiou, A.; Greig, N.; Kamal, M. Biomarkers for Alzheimer's Disease Diagnosis. *Curr. Alzheimer Res.* **2017**, *14*, 1.
(9) Zetterberg, H.; Andreasson, U.; Hansson, O.; Wu, G.; Sankaranarayanan, S.; Andersson, M. E.; Buchhave, P.; Londos, E.; Umek, R. M.; Minthon, L.; et al. Elevated Cerebrospinal Fluid BACE1 Activity in Incipient Alzheimer Disease. *Arch. Neurol.* **2008**, *65*, 1102−1107.
(10) Du, Y.; Dodel, R.; Hampel, H.; Buerger, K.; Lin, S.; Eastwood, B.; Bales, K.; Gao, F.; Moeller, H.-J.; Oertel, W.; et al. Reduced Levels of Amyloid β-Peptide Antibody in Alzheimer Disease. *Neurology* **2001**, *57*, 801−805.
(11) Kanai, M.; Matsubara, E.; Isoe, K.; Urakami, K.; Nakashima, K.; Arai, H.; Sasaki, H.; Abe, K.; Iwatsubo, T.; Kosaka, T.; et al. Longitudinal Study of Cerebrospinal Fluid Levels of Tau, A Beta1-40, and A Beta1-42(43) in Alzheimer's Disease: A Study in Japan. *Ann. Neurol.* **1998**, *44*, 17−26.
(12) Hampel, H.; Blennow, K. CSF Tau and β-Amyloid as Biomarkers for Mild Cognitive Impairment. *Dialogues Clin. Neurosci.* **2004**, *6*, 379−390.
(13) Sui, X.; Liu, J.; Yang, X. Cerebrospinal Fluid Biomarkers of Alzheimer's Disease. *Neurosci. Bull.* **2014**, *30*, 233−242.
(14) Kuhlmann, J.; Andreasson, U.; Pannee, J.; Bjerke, M.; Portelius, E.; Leinenbach, A.; Bittner, T.; Korecka, M.; Jenkins, R. G.; Vanderstichele, H.; et al. CSF Aβ1−42− an Excellent but Complicated Alzheimer's Biomarker − a Route to Standardisation. *Clin. Chim. Acta* **2017**, *467*, 27−33.
(15) Ghasemi, F.; Hormozi-Nezhad, M. R.; Mahmoudi, M. Label-Free Detection of β-Amyloid Peptides (Aβ40 and Aβ42): A Colorimetric Sensor Array for Plasma Monitoring of Alzheimer's Disease. *Nanoscale* **2018**, *10*, 6361−6368.
(16) Zhao, Z.; Zhu, L.; Bu, X.; Ma, H.; Yang, S.; Yang, Y.; Hu, Z. Label-Free Detection of Alzheimer's Disease through the ADP3 Peptoid Recognizing the Serum Amyloid-Beta42 Peptide. *Chem. Commun.* **2015**, *51*, 718−721.
(17) Cheng, X. R.; Hau, B. Y. H.; Veloso, A. J.; Martic, S.; Kraatz, H.-B.; Kerman, K. Surface Plasmon Resonance Imaging of Amyloid-?? Aggregation Kinetics in the Presence of Epigallocatechin Gallate and Metals. *Anal. Chem.* **2013**, *85*, 2049−2055.
(18) Oh, J.; Yoo, G.; Chang, Y. W.; Kim, H. J.; Jose, J.; Kim, E.; Pyun, J.-C.; Yoo, K.-H. A Carbon Nanotube Metal Semiconductor Field Effect Transistor-Based Biosensor for Detection of Amyloid-Beta in Human Serum. *Biosens. Bioelectron.* **2013**, *50*, 345−350.
(19) Prabhulkar, S.; Piatyszek, R.; Cirrito, J. R.; Wu, Z.-Z.; Li, C.-Z. Microbiosensor for Alzheimer's Disease Diagnostics: Detection of Amyloid Beta Biomarkers. *J. Neurochem.* **2012**, *122*, 374−381.
(20) Yoo, Y. K.; Kim, J.; Kim, G.; Kim, Y. S.; Kim, H. Y.; Lee, S.; Cho, W. W.; Kim, S.; Lee, S.-M.; Lee, B. C.; et al. A Highly Sensitive Plasma-Based Amyloid-β Detection System through Medium-Changing and Noise Cancellation System for Early Diagnosis of the Alzheimer's Disease. *Sci. Rep.* **2017**, *7*, 1−10.
(21) Couto, R. A. S.; Lima, J. L. F. C.; Quinaz, M. B. Recent Developments, Characteristics and Potential Applications of Screen-Printed Electrodes in Pharmaceutical and Biological Analysis. *Talanta* **2016**, *146*, 801−814.
(22) Xia, N.; Zhang, Y.; Guan, P.; Hao, Y.; Liu, L. A Simple and Label-Free Electrochemical Method for Detection of Beta-Site Amyloid Precursor Protein Cleaving Enzyme and Screening of Its Inhibitor. *Sens. Actuators, B* **2015**, *213*, 111−115.
(23) Alarcón-Ángeles, G.; Guix, M.; Silva, W. C.; Ramírez-Silva, M. T.; Palomar-Pardavé, M.; Romero-Romo, M.; Merkoçi, A. Enzyme Entrapment by β-Cyclodextrin Electropolymerization onto a Carbon Nanotubes-Modified Screen-Printed Electrode. *Biosens. Bioelectron.* **2010**, *26*, 1768−1773.
(24) Fujii, S.; Sono, D.; Matsubara, K.; Abe, H. Electrochemical Quantification of the Alzheimer's Disease Amyloid-β (1-40) Using Amyloid-β Fibrillization Promoting Peptide. *Sens. Bio-Sens. Res.* **2015**, *6*, 7−12.
(25) Vestergaard, M.; Kerman, K.; Saito, M.; Nagatani, N.; Takamura, Y.; Tamiya, E. A Rapid Label-Free Electrochemical Detection and Kinetic Study of Alzheimer's Amyloid Beta Aggregation. *J. Am. Chem. Soc.* **2005**, *127*, 11892−11893.
(26) Qu, F.; Yang, M.; Rasooly, A. Dual Signal Amplification Electrochemical Biosensor for Monitoring the Activity and Inhibition of the Alzheimer's Related Protease β-Secretase. *Anal. Chem.* **2016**, *88*, 10559−10565.
(27) Haes, A. J.; Chang, L.; Klein, W. L.; Van Duyne, R. P. Detection of a Biomarker for Alzheimer's Disease from Synthetic and Clinical Samples Using a Nanoscale Optical Biosensor. *J. Am. Chem. Soc.* **2005**, *127*, 2264−2271.
(28) Liu, L.; He, Q.; Zhao, F.; Xia, N.; Liu, H.; Li, S.; Liu, R.; Zhang, H. Competitive Electrochemical Immunoassay for Detection of β-Amyloid (1-42) and Total β-Amyloid Peptides Using p-Aminophenol Redox Cycling. *Biosens. Bioelectron.* **2014**, *51*, 208−212.
(29) Rama, E. C.; González-García, M. B.; Costa-García, A. Competitive Electrochemical Immunosensor for Amyloid-Beta 1-42 Detection Based on Gold Nanostructurated Screen-Printed Carbon Electrodes. *Sens. Actuators, B* **2014**, *201*, 567−571.
(30) Crivianu-Gaita, V.; Thompson, M. Aptamers, Antibody ScFv, and Antibody Fab' Fragments: An Overview and Comparison of Three of the Most Versatile Biosensor Biorecognition Elements. *Biosens. Bioelectron.* **2016**, *85*, 32−45.
(31) Bossi, A.; Bonini, F.; Turner, A. P. F.; Piletsky, S. A. Molecularly Imprinted Polymers for the Recognition of Proteins: The State of the Art. *Biosens. Bioelectron.* **2007**, *22*, 1131−1137.

https://dx.doi.org/10.1021/acsomega.0c00062
ACS Omega 2020, 5, 12057−12066

(32) Martins, G. V.; Marques, A. C.; Fortunato, E.; Sales, M. G. F. 8-Hydroxy-2'-Deoxyguanosine (8-OHdG) Biomarker Detection down to PicoMolar Level on a Plastic Antibody Film. *Biosens. Bioelectron.* **2016**, *86*, 225−234.
(33) Gomes, R. S.; Moreira, F. T. C.; Fernandes, R.; Sales, M. G. F. Sensing CA 15-3 in Point-of-Care by Electropolymerizing O-Phenylenediamine (OPDA) on Au-Screen Printed Electrodes. *PLoS One* **2018**, *13*, No. e0196656.
(34) Erdőssy, J.; Horváth, V.; Yarman, A.; Scheller, F. W.; Gyurcsányi, R. E. Electrosynthesized Molecularly Imprinted Polymers for Protein Recognition. *TrAC, Trends Anal. Chem.* **2016**, *79*, 179−190.
(35) Cardoso, A. R.; Tavares, A. P. M.; Sales, M. G. F. In-Situ Generated Molecularly Imprinted Material for Chloramphenicol Electrochemical Sensing in Waters down to the Nanomolar Level. *Sens. Actuators, B* **2018**, *256*, 420−428.
(36) Moreira, F. T. C.; Sales, M. G. F. Smart Naturally Plastic Antibody Based on Poly(α-Cyclodextrin) Polymer for β-Amyloid-42 Soluble Oligomer Detection. *Sens. Actuators, B* **2017**, *240*, 229−238.
(37) Emam, S.; Adedoyin, A.; Geng, X.; Zaeimbashi, M.; Adams, J.; Ekenseair, A.; Podlaha-Murphy, E.; Sun, N. X. A Molecularly Imprinted Electrochemical Gas Sensor to Sense Butylated Hydroxytoluene in Air. *J. Sens.* **2018**, *2018*, 1−9.
(38) Reddy, A. S. G.; Narakathu, B. B.; Atashbar, M. Z.; Rebros, M.; Hrehorova, E.; Joyce, M. Printed Electrochemical Based Biosensors on Flexible Substrates. *Proceedings IEEE Sensors*, 2010; pp 1596−1600.
(39) Moreira, F. T. C.; Ferreira, M. J. M. S.; Puga, J. R. T.; Sales, M. G. F. Screen-Printed Electrode Produced by Printed-Circuit Board Technology. Application to Cancer Biomarker Detection by Means of Plastic Antibody as Sensing Material. *Sens. Actuators, B* **2016**, *223*, 927−935.
(40) Liu, H.; Zhou, X.; Shen, Q.; Xing, D. Paper-Based Electrochemiluminescence Sensor for Highly Sensitive Detection of Amyloid-β Oligomerization: Toward Potential Diagnosis of Alzheimer's Disease. *Theranostics* **2018**, *8*, 2289−2299.
(41) Irimia-Vladu, M. Green" Electronics: Biodegradable and Biocompatible Materials and Devices for Sustainable Future. *Chem. Soc. Rev.* **2014**, *43*, 588−610.
(42) Jin, J.-H.; Kim, J.; Lee, S.; Choi, S.; Park, C.; Min, N. A Fully Integrated Paper-Microfluidic Electrochemical Device for Simultaneous Analysis of Physiologic Blood Ions. *Sensors* **2018**, *18*, 104.
(43) Shafiee, H.; Asghar, W.; Inci, F.; Yuksekkaya, M.; Jahangir, M.; Zhang, M. H.; Durmus, N. G.; Gurkan, U. A.; Kuritzkes, D. R.; Demirci, U. Paper and Flexible Substrates as Materials for Biosensing Platforms to Detect Multiple Biotargets. *Sci. Rep.* **2015**, *5*, 8719.
(44) Ferreira, N. S.; Moreira, A. P. T.; de Sá, M. H. M.; Sales, M. G. F. New Electrochemically-Derived Plastic Antibody on a Simple Conductive Paper Support for Protein Detection: Application to BSA. *Sens. Actuators, B* **2017**, *243*, 1127−1136.
(45) Khan, S.; Lorenzelli, L.; Dahiya, R. S. Technologies for Printing Sensors and Electronics over Large Flexible Substrates: A Review. *IEEE Sens. J.* **2015**, *15*, 3164−3185.
(46) Tobjörk, D.; Österbacka, R. Paper Electronics. *Adv. Mater.* **2011**, *23*, 1935−1961.
(47) Marques, A. C.; Santos, L.; Costa, M. N.; Dantas, J. M.; Duarte, P.; Gonçalves, A.; Martins, R.; Salgueiro, C. A.; Fortunato, E. Office Paper Platform for Bioelectrochromic Detection of Electrochemically Active Bacteria Using Tungsten Trioxide Nanoprobes. *Sci. Rep.* **2015**, *5*, 9910.
(48) Costa, M. N.; Veigas, B.; Jacob, J. M.; Santos, D. S.; Gomes, J.; Baptista, P. V.; Martins, R.; Inácio, J.; Fortunato, E. A Low Cost, Safe, Disposable, Rapid and Self-Sustainable Paper-Based Platform for Diagnostic Testing: Lab-on-Paper. *Nanotechnology* **2014**, *25*, 094006.
(49) Purushothama, H. T.; Nayaka, Y. A.; Vinay, M. M.; Manjunatha, P.; Yathisha, R. O.; Basavarajappa, K. V. Pencil Graphite Electrode as an Electrochemical Sensor for the Voltammetric Determination of Chlorpromazine. *J. Sci. Adv. Mater. Devices* **2018**, *3*, 161−166.
(50) Gong, Z. Q.; Sujari, A. N. A.; Ab Ghani, S. Electrochemical Fabrication, Characterization and Application of Carboxylic Multi-Walled Carbon Nanotube Modified Composite Pencil Graphite Electrodes. *Electrochim. Acta* **2012**, *65*, 257−265.
(51) Phillips, C.; Al-Ahmadi, A.; Potts, S.-J.; Claypole, T.; Deganello, D. The Effect of Graphite and Carbon Black Ratios on Conductive Ink Performance. *J. Mater. Sci.* **2017**, *52*, 9520−9530.
(52) Wallace, G. G.; Teasdale, P. R.; Geoffrey, M.; Spinks, L. A. P. K.-M. *Conductive Electroactive Polymers: Intelligent Polymer Systems*, 3rd ed.; CRC Press, 2008.
(53) Ferrari, A. C. Raman Spectroscopy of Graphene and Graphite: Disorder, Electron-Phonon Coupling, Doping and Nonadiabatic Effects. *Solid State Commun.* **2007**, *143*, 47−57.
(54) Withers, F.; Russo, S.; Dubois, M.; Craciun, M. F. Tuning the Electronic Transport Properties of Graphenme through Functionalisation with Fluorine. *Nanoscale Res. Lett.* **2011**, *6*, 526.
(55) Luo, Z.; Yu, T.; Ni, Z.; Lim, S.; Hu, H.; Shang, J.; Liu, L.; Shen, Z.; Lin, J. Electronic Structures and Structural Evolution of Hydrogenated Graphene Probed by Raman Spectroscopy. *J. Phys. Chem. C* **2011**, *115*, 1422−1427.
(56) Tavares, A. P. M.; Sales, M. G. F. Novel Electro-Polymerized Protein-Imprinted Materials Using Eriochrome Black T: Application to BSA Sensing. *Electrochim. Acta* **2018**, *262*, 214−225.
(57) Irizarry, M. C. Biomarkers of Alzheimer Disease in Plasma. *NeuroRx* **2004**, *1*, 226−234.
(58) Gobbi, M.; Re, F.; Canovi, M.; Beeg, M.; Gregori, M.; Sesana, S.; Sonnino, S.; Brogioli, D.; Musicanti, C.; Gasco, P.; et al. Lipid-Based Nanoparticles with High Binding Affinity for Amyloid-B1-42 Peptide. *Biomaterials* **2010**, *31*, 6519−6529.
(59) Carneiro, M. C. C. G.; Moreira, F. T. C.; Dutra, R. A. F.; Fernandes, R.; Sales, M. G. F. Homemade 3-Carbon Electrode System for Electrochemical Sensing: Application to MicroRNA Detection. *Microchem. J.* **2018**, *138*, 35−44.

https://dx.doi.org/10.1021/acsomega.0c00062
ACS Omega 2020, 5, 12057−12066